Supporting Information for

The Formation and Stability of Fluoxetine HCl Cocrystals Investigated by Multicomponent Milling

Austin A. Peach[1,2], Sean T. Holmes[1,2], Leonard R. MacGillivray[3], and Robert W. Schurko[1,2,*]
1. Department of Chemistry and Biochemistry, Florida State University, Tallahassee, FL 32306
2. National High Magnetic Field Laboratory, Tallahassee, FL 32310
3. Department of Chemistry and Biochemistry, University of Iowa, Iowa City, IA 52242
*Author to whom correspondence should be addressed. E-mail: rschurko@fsu.edu; Web: https://www.chem.fsu.edu/~schurko/; Tel: 850-645-8614

Table of Contents:

Figure Column with Title:	Page #
Table S1: Mechanochemical and slow evaporation synthesis parameters for competitive reactions.	3
Table S2: Mechanochemical and slow evaporation synthesis parameters for stability reactions.	4
Table S3: ^{35}Cl{^{1}H} static CPMG SSNMR acquisition parameters for experiments conducted at 18.8 T on samples from all CM and SM experiments.	5
Table S4: ^{35}Cl{^{1}H} static CPMG SSNMR acquisition parameters for experiments conducted at 18.8 T on a sample of **X**, **XB**, **X$_2$F**, **X$_2$S**.	6
Table S5: ^{1}H-^{13}C VACP/MAS SSNMR acquisition parameters for experiments conducted at 14.1 T on a sample of **X**, **XB**, **X$_2$F**, **X$_2$S**.	7
Table S6: ^{1}H-^{13}C VACP/MAS SSNMR acquisition parameters for experiments conducted at 14.1 T on a sample of fumaric acid, succinic acid, and benzoic acid.	8
Table S7: ^{1}H-^{13}C VACP/MAS SSNMR acquisition parameters for experiments conducted at 14.1 T on a sample from all CM and SM reactions.	9
Table S8. Experimental and calculated ^{35}Cl EFG and CS tensor parameters for **X**, **X$_2$F**, **XB**, and **X$_2$S**.[a]	10
Table S9. Precise and rounded integrated intensities for competitive and stability milling reactions with mixed products.	11
Table S10. DFT-D2* static lattice energies of crystal structures of benzoic and succinic acid acquired at varying temperatures.	12
Figure S1. ^{1}H-^{13}C CP/MAS (ν_{rot} = 10 kHz) SSNMR spectra acquired at B_0 = 14.1 T of **B** (green), **F** (red), and **S** (purple). Dashed lines correspond to the unique ^{13}C chemical shifts of each carboxylic acid. The dashed line in black is a shared ^{13}C chemical shift between **F** and **B**. Spinning sidebands are indicated with asterisks (*).	13
Figure S2. ^{1}H-^{13}C CP/MAS (ν_{rot} = 10 kHz) SSNMR spectra acquired at B_0 = 14.1 T of **X** (blue), **XB** (green), **X$_2$F** (red), and **X$_2$S** (purple). Dashed lines correspond to the unique ^{13}C chemical shifts of **X**, **XB**, **X$_2$F**, and **X$_2$S**. Spinning sidebands are indicated with asterisks (*).	14
Figure S3. ^{1}H-^{13}C CP/MAS (ν_{rot} = 10 kHz) SSNMR spectra acquired at B_0 = 14.1 T of (**i**) **X** (blue), **B** (black), and **XB** (green). Dashed lines correspond to the unique ^{13}C chemical shifts of **X**, **B**, and **XB**. Spinning sidebands are indicated with asterisks (*).	15
Figure S4. ^{1}H-^{13}C CP/MAS (ν_{rot} = 10 kHz) SSNMR spectra acquired at B_0 = 14.1 T of **X** (blue), **F** (black), and **X$_2$F** (red). Dashed lines correspond to the unique ^{13}C chemical shifts of **X**, **F**, and **X$_2$F**. Spinning sidebands are indicated with asterisks (*).	16
Figure S5. ^{1}H-^{13}C CP/MAS (ν_{rot} = 10 kHz) SSNMR spectra acquired at B_0 = 14.1 T of **X** (blue), **F** (black), and **X$_2$S** (purple). Dashed lines correspond to the unique ^{13}C chemical shifts of **X**, **S**, and **X$_2$S**. Spinning sidebands are indicated with asterisks (*).	17
Figure S6. ^{1}H-^{13}C CP/MAS (ν_{rot} = 10 kHz) SSNMR spectra acquired at B_0 = 14.1 T of CM1, CM2, and CM4 (black), **S** (purple), **F** (red), and **XB** (green). Dashed lines correspond to the unique ^{13}C chemical shifts of **X**, **S**, and **XB**, respectively; this supports the formation of the **XB** PCC and unreacted educts **S** and **F**. Spinning sidebands are indicated with asterisks (*).	18

Figure S7. ^{1}H-^{13}C CP/MAS (ν_{rot} = 10 kHz) SSNMR spectra acquired at B_0 = 14.1 T of CM3 (black), $\mathbf{X_2F}$ (red), and $\mathbf{X_2S}$ (purple). Dashed lines correspond to the unique ^{13}C chemical shifts between $\mathbf{X_2F}$ and $\mathbf{X_2S}$, demonstrating that both PCCs are formed and there is no excess **X**. Spinning sidebands are indicated with asterisks (*).	19
Figure S8. ^{1}H-^{13}C CP/MAS (ν_{rot} = 10 kHz) SSNMR spectra acquired at B_0 = 14.1 T of CM9, CM10, and CM11 (black), $\mathbf{X_2F}$ (red), and $\mathbf{X_2S}$ (purple). Dashed lines correspond to the unique ^{13}C chemical shifts of $\mathbf{X_2F}$ and $\mathbf{X_2S}$; this supports the formation of both PCCs. Spinning sidebands are indicated with asterisks (*).	20
Figure S9. FIDs of ^{35}Cl CPMG spectra acquired at B_0 = 18.8 T of **X**, **XB**, $\mathbf{X_2F}$, and $\mathbf{X_2S}$ used for the determination of T_2^{eff}(^{35}Cl) (*cf.* **Table S4**).	21
Figure S10. ^{35}Cl{^{1}H} CPMG SSNMR spectra acquired at B_0 = 18.8 T with deconvolutions of CM1, CM2, CM3, and CM4 for extended milling times of 90 minutes (left) and slow evaporation over ten days (right). Deconvolutions (**X** = blue, **XB** = green, $\mathbf{X_2F}$ = red, $\mathbf{X_2S}$ = purple, and $\mathbf{X_2F}$+$\mathbf{X_2S}$ = orange, **X**+$\mathbf{X_2F}$+$\mathbf{X_2S}$ = brown) indicate the product(s) of each reaction. In the case of CM1, CM2, and CM4 the reaction results in the **XB** PCC. In CM3 for the extended milling times the reaction results in a mix of $\mathbf{X_2F}$ and $\mathbf{X_2S}$ PCCs, whereas in the slow evaporation syntheses there is the presence of unreacted **X**.	22
Figure S11. ^{1}H-^{13}C CP/MAS (ν_{rot} = 10 kHz) SSNMR spectra acquired at B_0 = 14.1 T of SM4 (black), $\mathbf{X_2F}$ (red), and $\mathbf{X_2S}$ (purple). Dashed lines correspond to the unique ^{13}C chemical shifts between $\mathbf{X_2F}$ and $\mathbf{X_2S}$, demonstrating that a stoichiometric amount of **S** has exchanged with **F**, forming $\mathbf{X_2S}$. Spinning sidebands are indicated with asterisks (*).	23
Figure S12. ^{1}H-^{13}C CP/MAS (ν_{rot} = 10 kHz) SSNMR spectra acquired at B_0 = 14.1 T of SM6 (black), $\mathbf{X_2F}$ (red), and $\mathbf{X_2S}$ (purple). Dashed lines correspond to the unique ^{13}C chemical shifts between $\mathbf{X_2F}$ and $\mathbf{X_2S}$, demonstrating that a stoichiometric amount of **F** has exchanged with **S**, forming $\mathbf{X_2F}$. Spinning sidebands are indicated with asterisks (*).	24
Figure S13. ^{35}Cl{^{1}H} CPMG SSNMR spectra acquired at B_0 = 18.8 T with deconvolutions of SM1, SM2, SM3, SM4, SM5, and SM6 for extended milling times of 90 minutes (left) and slow evaporation over ten days (right). Deconvolutions (**XB** = green, $\mathbf{X_2F}$ = red, $\mathbf{X_2S}$ = purple, and $\mathbf{X_2F}$+$\mathbf{X_2S}$ = orange) indicate the product(s) of each reaction. In the case of SM1, SM2, SM4, and SM5 the reaction results in the **XB** PCC. In SM4 and SM6 the reaction results in a mix of $\mathbf{X_2F}$ and $\mathbf{X_2S}$ PCCs.	25
Supplement S1: DFT calculations	26
References	27

Tables

Table S1: Mechanochemical and slow evaporation synthesis parameters for competitive reactions.

	X		**B**		**F**		**S**	
Reaction[a]	mass (mg)	molar ratio	mass (mg)	molar ratio	mass (mg)	molar ratio	mass (mg)	molar ratio
CM1	70	2	25	2	--	--	12	1
CM2	70	2	25	2	12	1	--	--
CM3	75	2	--	--	13	1	13	1
CM4	70	2	25	2	12	1	12	1
CM5	80	4	14	2	--	--	7	1
CM6	80	8	22	6	--	--	4	1
CM7	80	8	7	2	--	--	10	3
CM8	90	6	10	2	--	--	5	1
CM9	90	4	--	--	8	1	8	1
CM10	90	8	--	--	4	1	12	3
CM11	90	8	--	--	12	3	4	1
CM12	90	6	--	--	5	1	5	1

[a] All reactions were performed by LAG and SE with 5 μL and 5 mL of ethanol, respectively. For LAG, educts were milled in a 10 mL jar with two 7 mm ball bearings, both stainless steel, and milled for 5 and 90 minutes at 30 Hz.

Table S2: Mechanochemical and slow evaporation synthesis parameters for stability reactions.

Reaction[a]	Initial Cocrystal	mass (mg)	molar ratio	Coformer	mass (mg)	molar ratio
SM1	**XB**	95	2	**F**	12	1
SM2	**XB**	95	2	**S**	12	1
SM3	**X_2F**	82	1	**B**	25	2
SM4	**X_2F**	82	1	**S**	12	1
SM5	**X_2S**	82	1	**B**	25	2
SM6	**X_2S**	82	1	**F**	12	1

[a] All reactions were performed by LAG and SE with 5 µL and 5 mL of ethanol, respectively. For LAG, educts were milled in a 10 mL jar with two 7 mm ball bearings, both stainless steel, and milled for 5 and 90 minutes at 30 Hz.

Table S3: $^{35}Cl\{^{1}H\}$ static CPMG SSNMR acquisition parameters for experiments conducted at 18.8 T on samples from all CM and SM experiments.

	Competitive Milling (CM1-CM4)	Competitive Milling (CM5-CM12)	Stability Milling (SM1-SM6)
Number of scans	14336	14336	14336
Experimental time (h)	4	4	4
Recycle delay (s)	1	1	1
^{35}Cl π/2 pulse width (μs)	5	5	5
^{35}Cl pulse rf (kHz)	50	50	50
Dwell (μs)	2	2	2
Number of echoes	30	30	30
Echo length (μs)	750	750	750
Spectral width (kHz)	250	250	250
Acquisition length (number of points)	13700	13700	13700
^{1}H decoupling field (kHz)	50	50	50

Table S4: $^{35}Cl\{^{1}H\}$ static CPMG SSNMR acquisition parameters for experiments conducted at 18.8 T on a sample of **X**, **XB**, **X_2F**, **X_2S**.

	X	**XB**	**X_2F**	**X_2S**
Number of scans	14336	14336	14336	14336
Experimental time (h)	4	4	4	4
Recycle delay (s)	1	1	1	1
^{35}Cl $\pi/2$ pulse width (μs)	5	5	5	5
^{35}Cl pulse rf (kHz)	50	50	50	50
Dwell (μs)	2	2	2	2
Number of echoes	30	30	30	30
Echo length (μs)	750	750	750	750
Spectral width (kHz)	250	250	250	250
Acquisition length (number of points)	13700	13700	13700	13700
^{1}H decoupling field (kHz)	50	50	50	50
T_2^{eff} (^{35}Cl, ms) [a]	8.5	13.5	10	14

[a] T_2^{eff} are determined using a monoexponential decay function of the form $a * \exp\left(-\frac{t}{T_2^{eff}}\right)$.

Table S5: ^{1}H-^{13}C VACP/MAS SSNMR acquisition parameters for experiments conducted at 14.1 T on a sample of **X**, **XB**, **X_2F**, **X_2S**.

	X	**XB**	**X_2F**	**X_2S**
Number of scans	512	512	512	256
Experimental time (h)	4	4	4	4
Recycle delay (s)	30	30	30	60
Contact time (ms)	1	1	1	1
^{1}H Hartmann-Hahn matching field (kHz)	50	50	50	50
^{1}H $\pi/2$ pulse width (μs)	2.5	2.5	2.5	2.5
Dwell (μs)				
Spectral width (ppm)	300	300	300	300
Acquisition length (number of points)	2048	2048	2048	2048
^{1}H decoupling field (kHz)	50	50	50	50
Spinning speed (kHz)	10	10	10	10

Table S6: ^{1}H-^{13}C VACP/MAS SSNMR acquisition parameters for experiments conducted at 14.1 T on a sample of fumaric acid, succinic acid, and benzoic acid.

	F	**B**	**S**
Number of scans	64	24	64
Experimental time (h)	2	2	2
Recycle delay (s)	120	300	120
Contact time (ms)	1	1	1
^{1}H Hartmann-Hahn matching field (kHz)	50	50	50
^{1}H $\pi/2$ pulse width (μs)	2.5	2.5	2.5
Dwell (μs)	11	11	11
Spectral width (ppm)	300	300	300
Acquisition length (number of points)	2048	2048	2048
^{1}H decoupling field (kHz)	50	50	50
Spinning speed (kHz)	10	10	10

Table S7: ^{1}H-^{13}C VACP/MAS SSNMR acquisition parameters for experiments conducted at 14.1 T on a sample from all CM and SM reactions.

	Competitive Milling (CM1 – CM12)	Stability Milling (SM1 – SM6)
Number of scans	512	512
Experimental time (h)	4	4
Recycle delay (s)	30	30
Contact time (ms)	1	1
^{1}H Hartmann-Hahn matching field (kHz)	50	50
^{1}H $\pi/2$ pulse width (μs)	2.5	2.5
Dwell (μs)	5	5
Spectral width (ppm)	300	300
Acquisition length (number of points)	2048	2048
^{1}H decoupling field (kHz)	50	50
Spinning speed (kHz)	10	10

Table S8. Experimental and calculated ^{35}Cl EFG and CS tensor parameters for **X**, **X$_2$F**, **XB**, and **X$_2$S**.[a]

		C_Q[b] (MHz)	η_Q[c]	δ_{iso} (ppm)[d]	Ω (ppm)[e]	κ[f]	α[g]	β[g]	γ[g]
X	Exp.	8.15(20)	0.26(3)	110(15)	36(13)	0.76(8)	130(180)	0(30)	275(180)
	rPBE-D2*	-7.73	0.30	84	123	-0.76	275	1	222
X$_2$F	Exp.	6.50(15)	0.28(4)	88(20)	104(15)	0.07(6)	145(20)	10(15)	205(20)
	rPBE-D2*	-6.70	0.17	69	113	-0.32	205	12	236
XB	Exp.	7.15(15)	0.23(3)	85(20)	121(10)	0.26(9)	220(30)	10(10)	125(30)
	rPBE-D2*[h]	-7.35	0.10	73	103	0.28	124	9	311
X$_2$S	Exp.	6.00(15)	0.21(2)	80(20)	121(15)	0.03(3)	30(25)	10(15)	345(20)
	rPBE-D2*	-6.48	0.14	59	96	-0.10	345	12	117

[a] Theoretically derived CS tensor parameters are presented only for the rPBE-D2* calculations (See **Supplement S1** for more details). The experimental uncertainty in the last digit(s) for each value is indicated in parentheses. [b] $C_Q = eQV_{33}/h$. The sign of C_Q cannot be determined from the experimental ^{35}Cl NMR spectra. [c] $\eta_Q = (V_{11} - V_{22})/V_{33}$. [d] $\delta_{iso} = (\delta_{11} + \delta_{22} + \delta_{33})/3$; [e] $\Omega = \delta_{11} - \delta_{33}$; [f] $\kappa = 3(\delta_{22} - \delta_{iso})/\Omega$. [g] The Euler angles α, β, and γ define the relative orientation of the CS and EFG tensors (*N.B.* ssNake uses the ZX'Z" convention). [h] Results are reported for one of the two crystallographically distinct chlorine sites, which have nearly identical chlorine NMR parameters.

Table S9. Precise and rounded integrated intensities for competitive and stability milling reactions with mixed products.

Reaction	Measured integrated intensities				Rounded integrated intensities [a]			
	X	**XB**	**X_2F**	**X_2S**	**X**	**XB**	**X_2F**	**X_2S**
CM3	-	-	1.3	1.0	-	-	1	1
CM5	-	2.2	-	1.1	-	2	-	1
CM6	-	5.7	-	1.2	-	6	-	1
CM7	-	1.9	-	3.2	-	2	-	3
CM8	2.1	2.1	-	0.9	2	2	-	1
CM9	-	-	1.1	1.0	-	-	1	1
CM10	-	-	1.2	3.1	-	-	1	3
CM11	-	-	3.1	1.2	-	-	3	1
CM12	2.2	-	1.1	1.1	2	-	1	1
SM4	-	-	1.1	0.9	-	-	1	1
SM6	-	-	1.1	0.9	-	-	1	1

[a] These rounded integrated intensities correspond to the known stoichiometries of corresponding CM and SM reactions (*cf.* Table 1 and 2) and are supported by NMR and pXRD data that do not reveal any impurities and are consistent with quantitative yields.

Table S10. DFT-D2* static lattice energies of crystal structures of benzoic and succinic acid acquired at varying temperatures.

Compound	Static Lattice Energy	120 K	150 K	180 K	283 K
Benzoic acid	Calculated (kJ/mol)	-201357.42	-201356.75	-201354.99	-201354.36
	Normalized (kJ/mol) [a]	0	0.67	2.43	3.06
Succinic acid	Calculated (kJ/mol)	-240557.34	-240557.16	-240557.04	-240555.11
	Normalized (kJ/mol)	0	0.18	0.30	2.23

[a] Normalized values are the difference between the static lattice energy at 120 K and the current temperature.

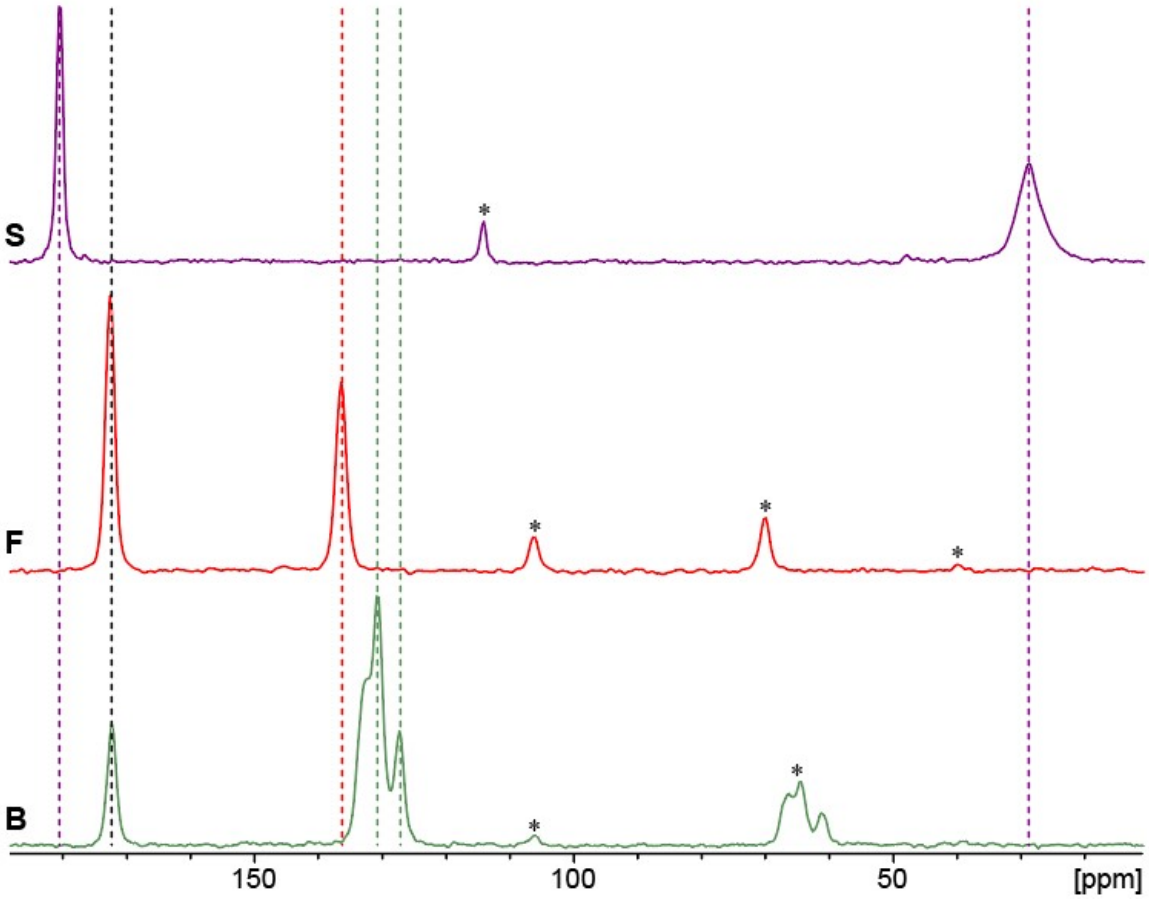

Figure S1. ^{1}H-^{13}C CP/MAS (ν_{rot} = 10 kHz) SSNMR spectra acquired at B_0 = 14.1 T of **B** (green), **F** (red), and **S** (purple). Dashed lines correspond to the unique ^{13}C chemical shifts of each carboxylic acid. The dashed line in black is a shared ^{13}C chemical shift between **F** and **B**. Spinning sidebands are indicated with asterisks (*).

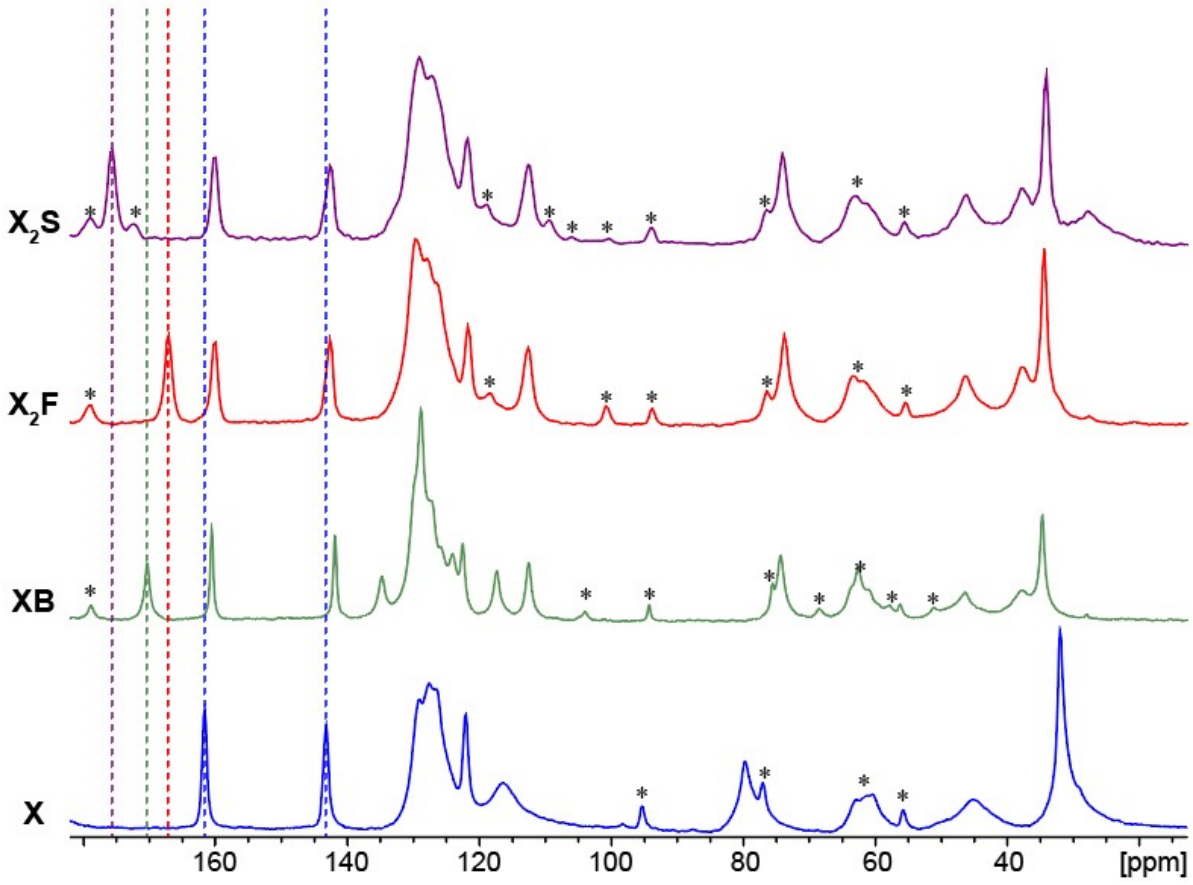

Figure S2. ^{1}H-^{13}C CP/MAS (ν_{rot} = 10 kHz) SSNMR spectra acquired at B_0 = 14.1 T of **X** (blue), **XB** (green), **X$_2$F** (red), and **X$_2$S** (purple). Dashed lines correspond to the unique ^{13}C chemical shifts of **X**, **XB**, **X$_2$F**, and **X$_2$S**. Spinning sidebands are indicated with asterisks (*).

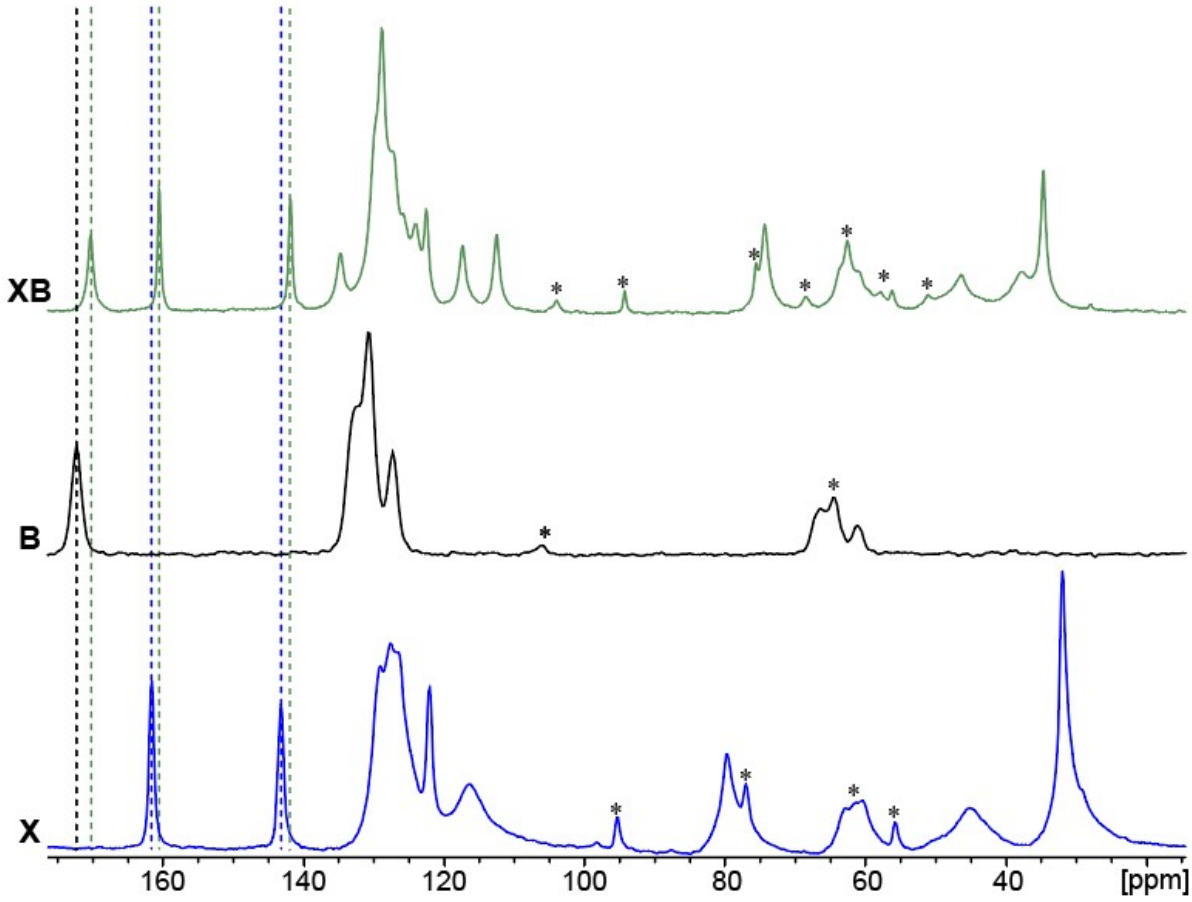

Figure S3. ^{1}H-^{13}C CP/MAS (ν_{rot} = 10 kHz) SSNMR spectra acquired at B_0 = 14.1 T of (**i**) **X** (blue), **B** (black), and **XB** (green). Dashed lines correspond to the unique ^{13}C chemical shifts of **X**, **B**, and **XB**. Spinning sidebands are indicated with asterisks (*).

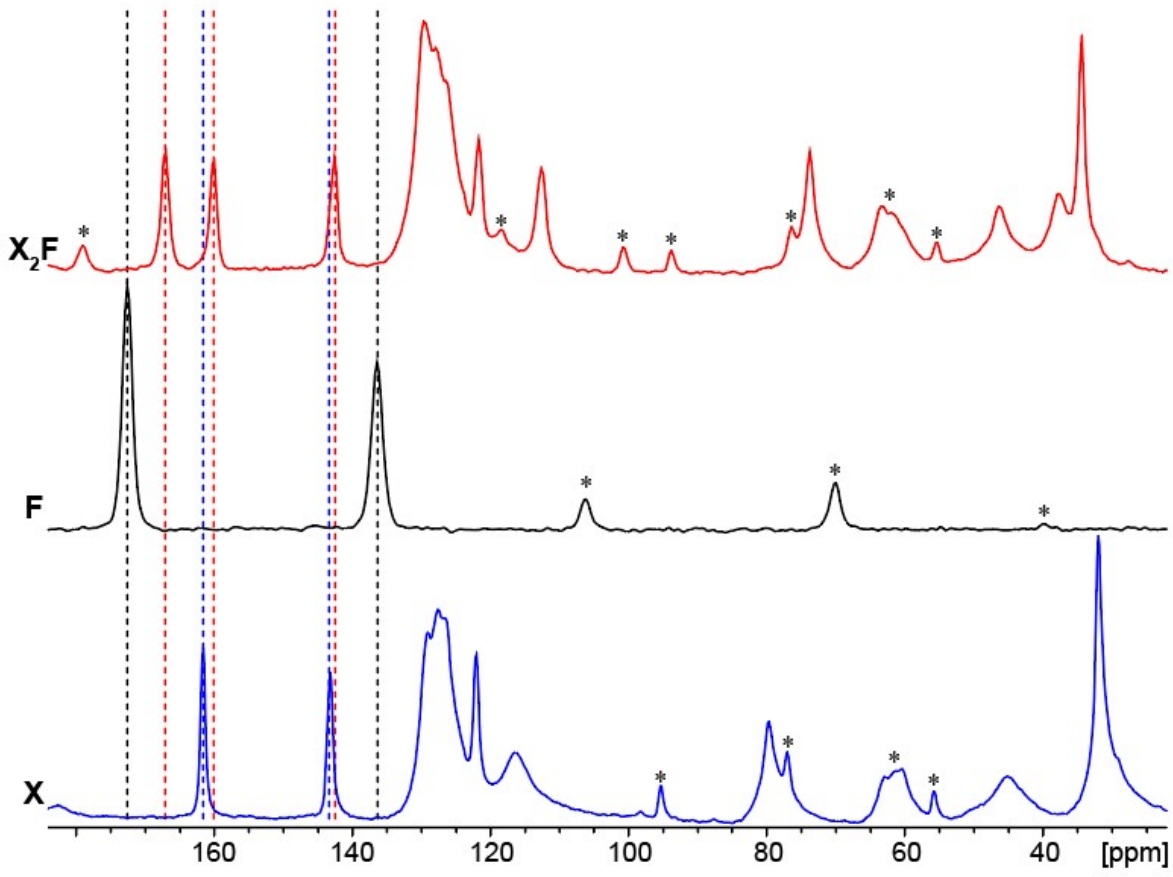

Figure S4. ^{1}H-^{13}C CP/MAS (ν_{rot} = 10 kHz) SSNMR spectra acquired at B_0 = 14.1 T of **X** (blue), **F** (black), and $\mathbf{X_2F}$ (red). Dashed lines correspond to the unique ^{13}C chemical shifts of **X**, **F**, and $\mathbf{X_2F}$. Spinning sidebands are indicated with asterisks (*).

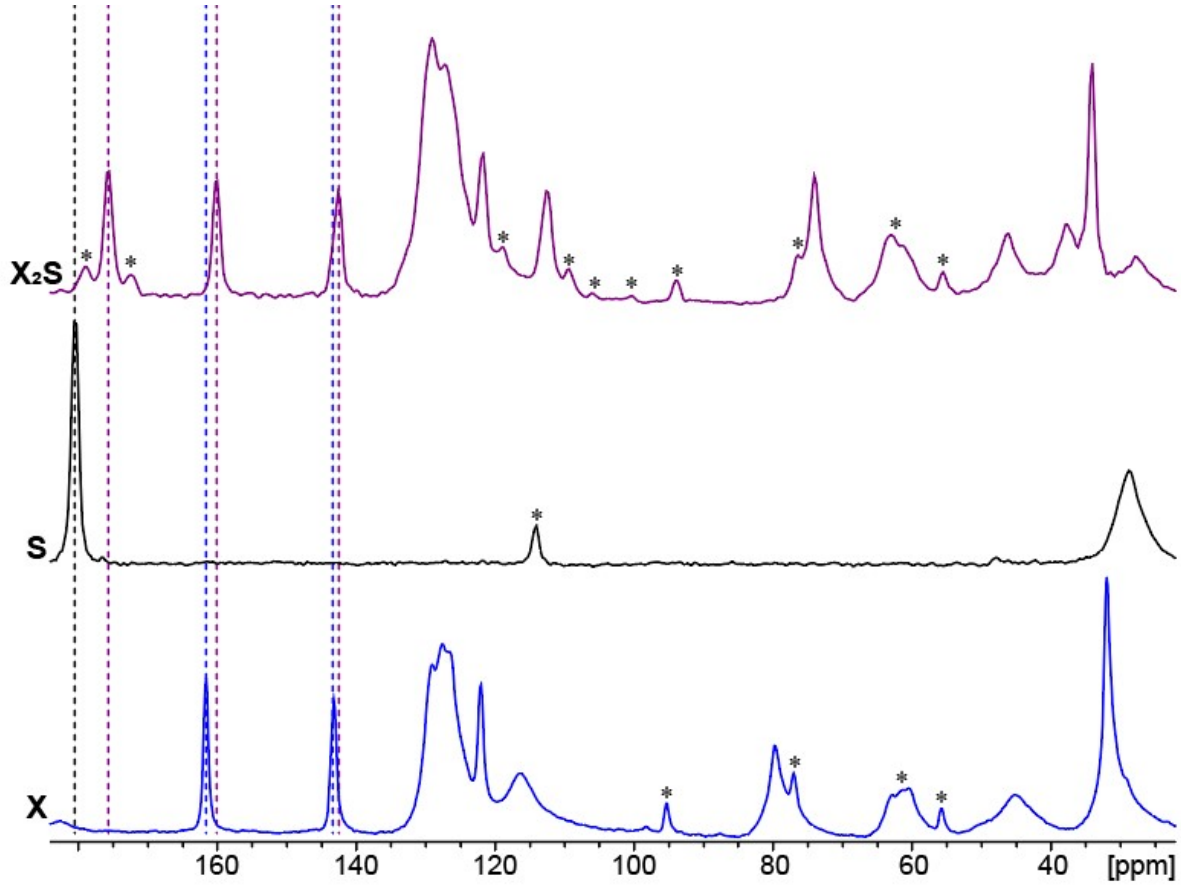

Figure S5. ^{1}H-^{13}C CP/MAS (ν_{rot} = 10 kHz) SSNMR spectra acquired at B_0 = 14.1 T of **X** (blue), **F** (black), and **X_2S** (purple). Dashed lines correspond to the unique ^{13}C chemical shifts of **X**, **S**, and **X_2S**. Spinning sidebands are indicated with asterisks (*).

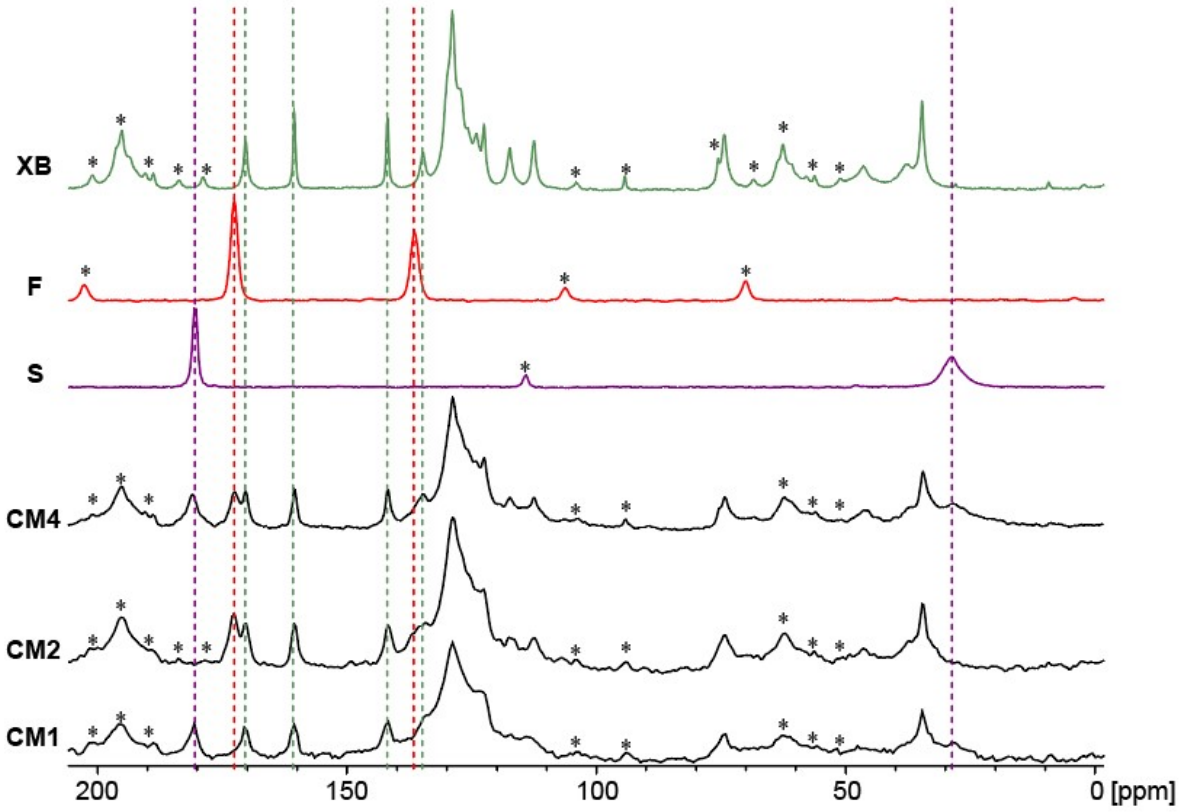

Figure S6. ^{1}H-^{13}C CP/MAS (ν_{rot} = 10 kHz) SSNMR spectra acquired at B_0 = 14.1 T of CM1, CM2, and CM4 (black), **S** (purple), **F** (red), and **XB** (green). Dashed lines correspond to the unique ^{13}C chemical shifts of **X**, **S**, and **XB**, respectively; this supports the formation of the **XB** PCC and unreacted educts **S** and **F**. Spinning sidebands are indicated with asterisks (*).

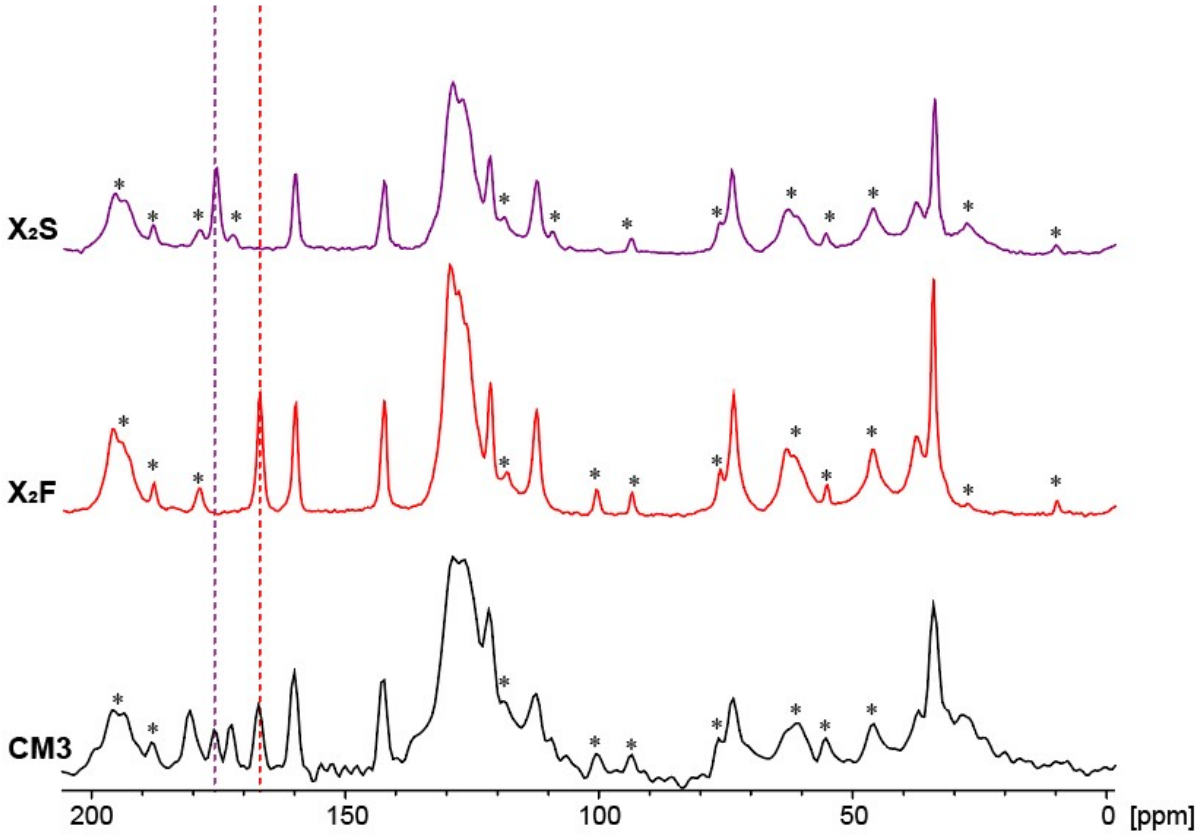

Figure S7. ^{1}H-^{13}C CP/MAS (ν_{rot} = 10 kHz) SSNMR spectra acquired at B_0 = 14.1 T of CM3 (black), **X_2F** (red), and **X_2S** (purple). Dashed lines correspond to the unique ^{13}C chemical shifts between **X_2F** and **X_2S**, demonstrating that both PCCs are formed and there is no excess **X**. Spinning sidebands are indicated with asterisks (*).

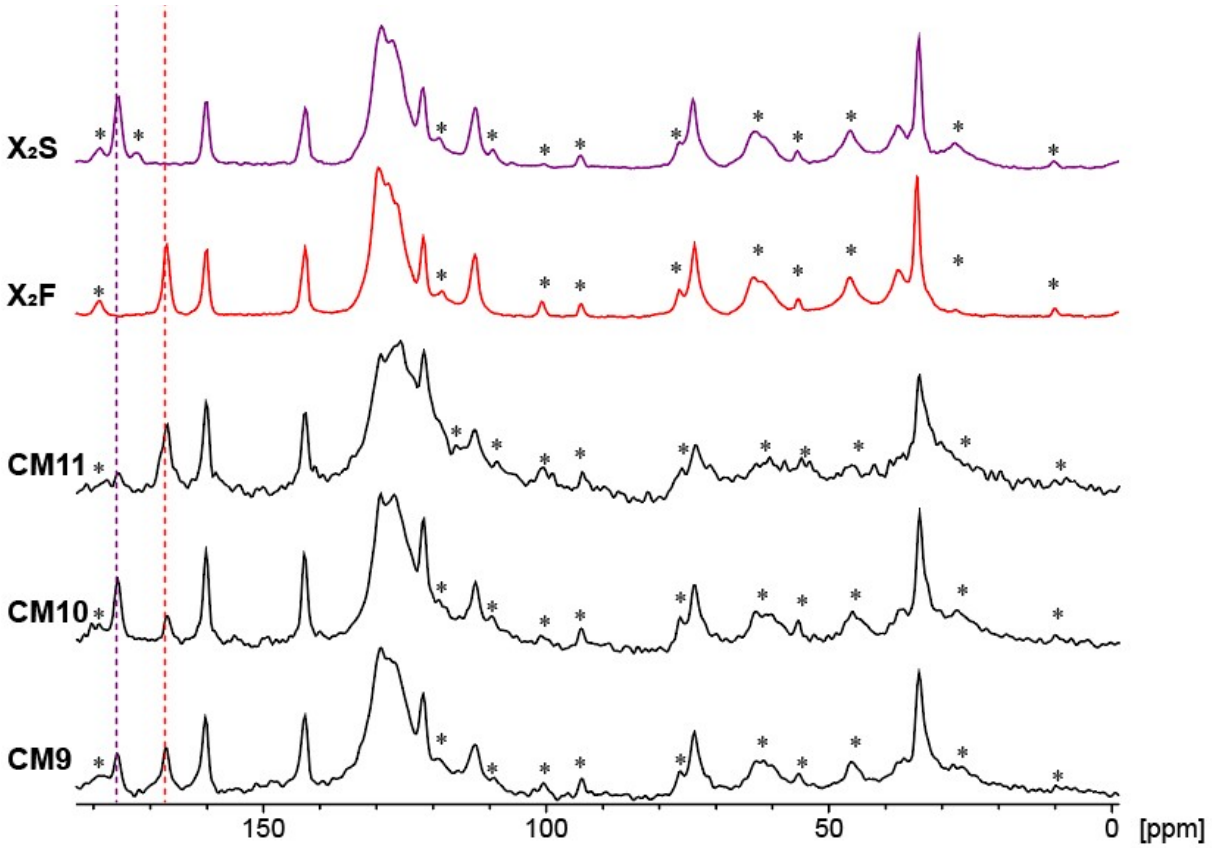

Figure S8. ^{1}H-^{13}C CP/MAS (ν_{rot} = 10 kHz) SSNMR spectra acquired at B_0 = 14.1 T of CM9, CM10, and CM11 (black), **X_2F** (red), and **X_2S** (purple). Dashed lines correspond to the unique ^{13}C chemical shifts of **X_2F** and **X_2S**; this supports the formation of both PCCs. Spinning sidebands are indicated with asterisks (*).

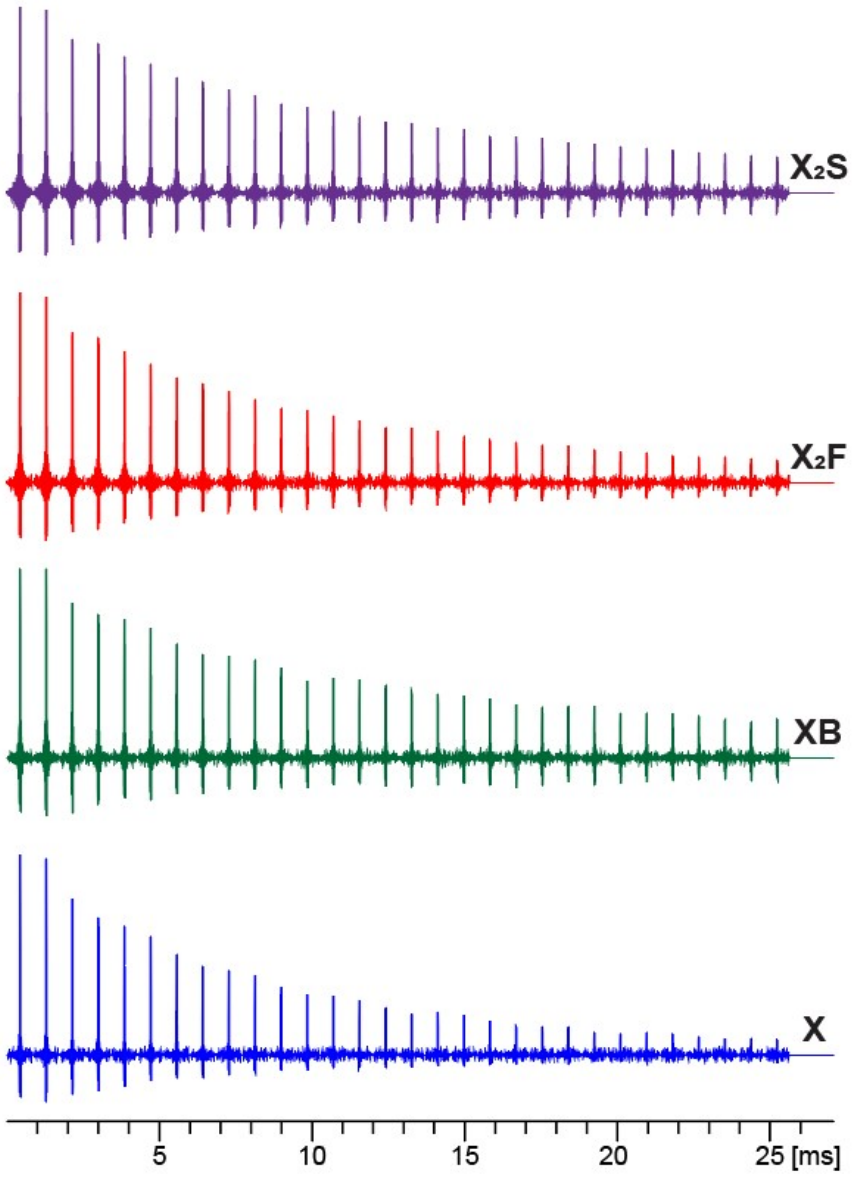

Figure S9. FIDs of ^{35}Cl CPMG spectra acquired at B_0 = 18.8 T of **X**, **XB**, **X$_2$F**, and **X$_2$S** used for the determination of $T_2^{\text{eff}}(^{35}\text{Cl})$ (*cf.* **Table S4**).

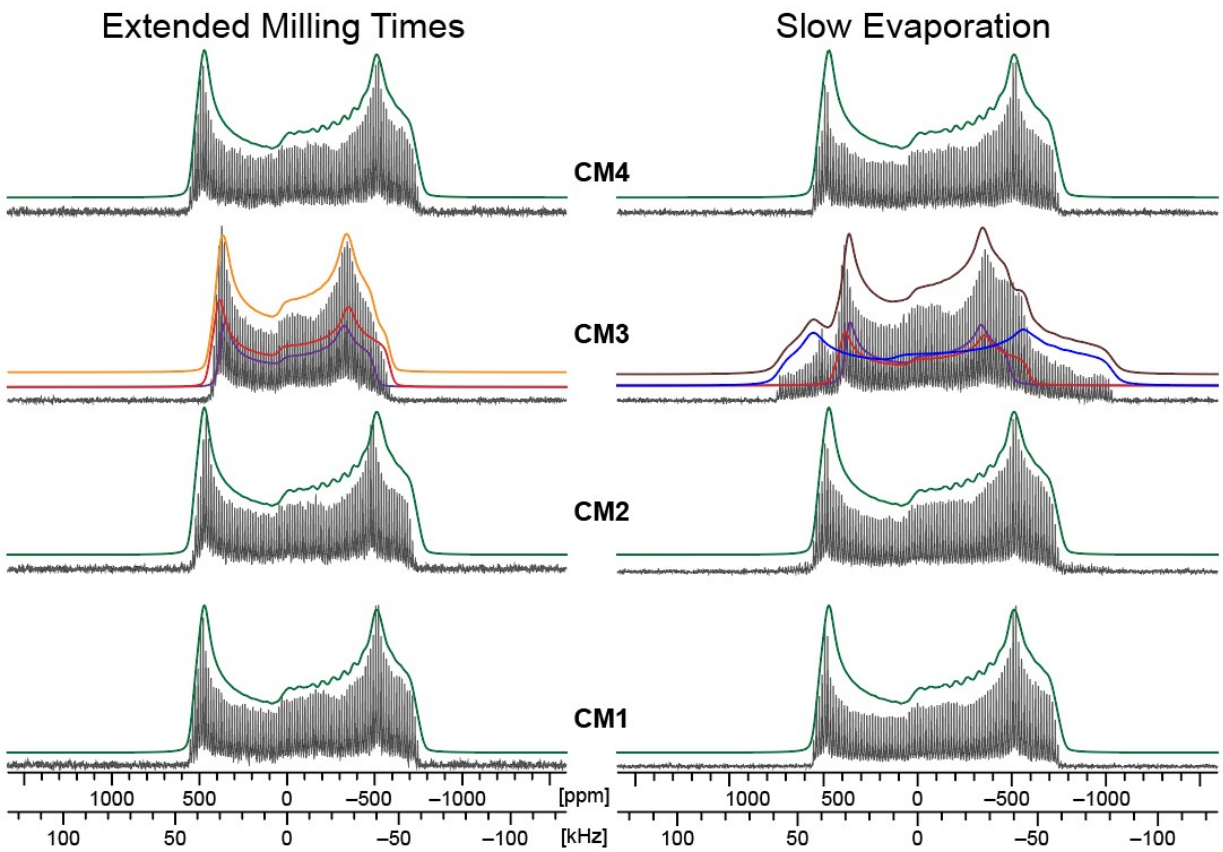

Figure S10. $^{35}Cl\{^{1}H\}$ CPMG SSNMR spectra acquired at B_0 = 18.8 T with deconvolutions of CM1, CM2, CM3, and CM4 for extended milling times of 90 minutes (left) and slow evaporation over ten days (right). Deconvolutions (**X** = blue, **XB** = green, $\mathbf{X_2F}$ = red, $\mathbf{X_2S}$ = purple, and $\mathbf{X_2F}$+$\mathbf{X_2S}$ = orange, **X**+$\mathbf{X_2F}$+$\mathbf{X_2S}$ = brown) indicate the product(s) of each reaction. In the case of CM1, CM2, and CM4 the reaction results in the **XB** PCC. In CM3 for the extended milling times the reaction results in a mix of $\mathbf{X_2F}$ and $\mathbf{X_2S}$ PCCs, whereas in the slow evaporation syntheses there is the presence of unreacted **X**.

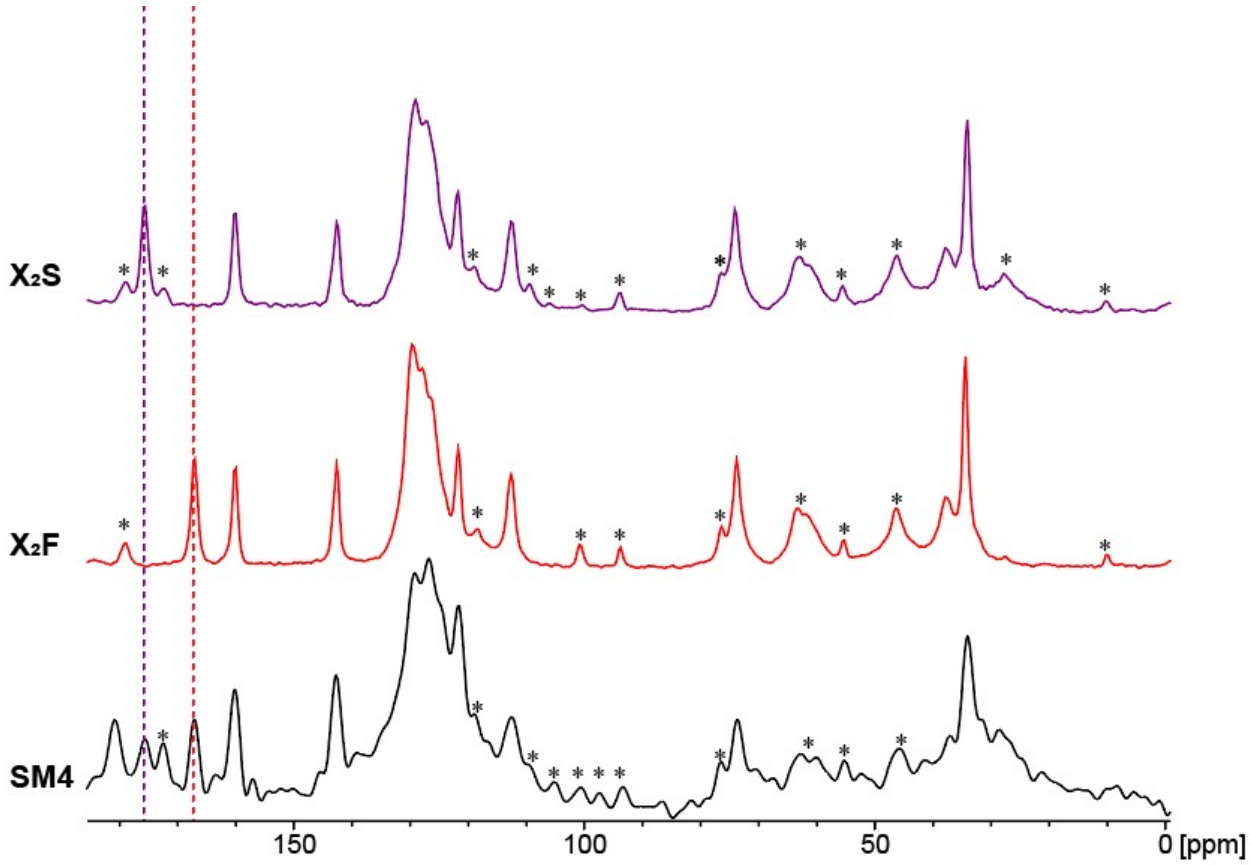

Figure S11. ^{1}H-^{13}C CP/MAS (ν_{rot} = 10 kHz) SSNMR spectra acquired at B_0 = 14.1 T of SM4 (black), **X_2F** (red), and **X_2S** (purple). Dashed lines correspond to the unique ^{13}C chemical shifts between **X_2F** and **X_2S**, demonstrating that a stoichiometric amount of **S** has exchanged with **F**, forming **X_2S.** Spinning sidebands are indicated with asterisks (*).

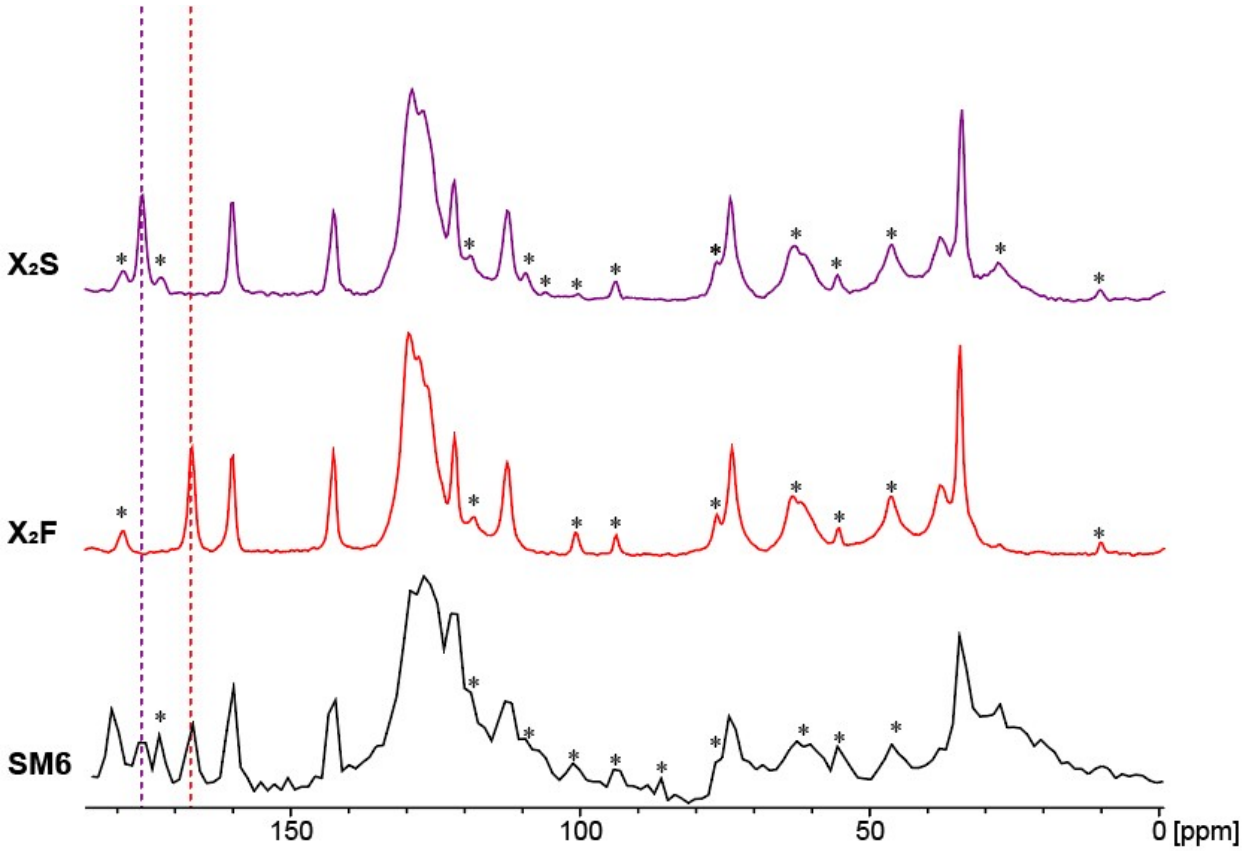

Figure S12. ^{1}H-^{13}C CP/MAS (ν_{rot} = 10 kHz) SSNMR spectra acquired at B_0 = 14.1 T of SM6 (black), **X$_2$F** (red), and **X$_2$S** (purple). Dashed lines correspond to the unique ^{13}C chemical shifts between **X$_2$F** and **X$_2$S**, demonstrating that a stoichiometric amount of **F** has exchanged with **S**, forming **X$_2$F.** Spinning sidebands are indicated with asterisks (*).

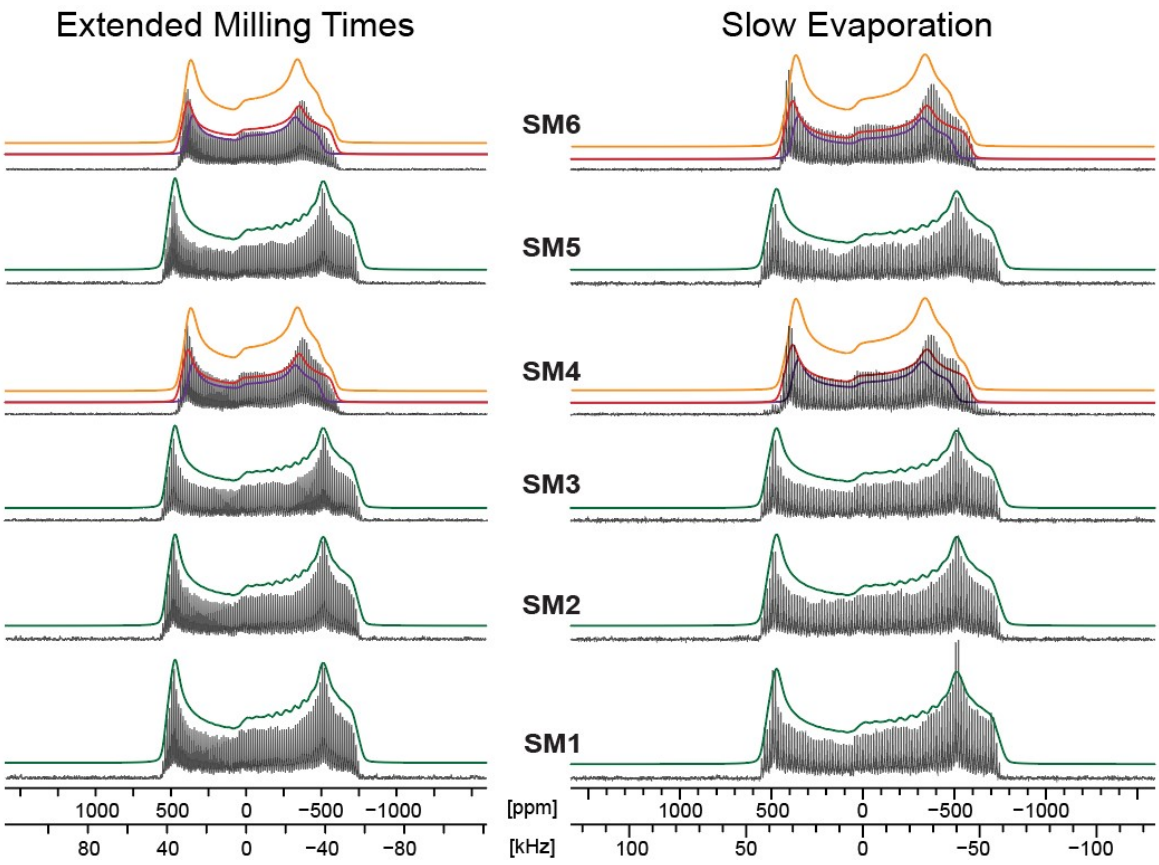

Figure S13. ^{35}Cl{^{1}H} CPMG SSNMR spectra acquired at B_0 = 18.8 T with deconvolutions of SM1, SM2, SM3, SM4, SM5, and SM6 for extended milling times of 90 minutes (left) and slow evaporation over ten days (right). Deconvolutions (**XB** = green, $\mathbf{X_2F}$ = red, $\mathbf{X_2S}$ = purple, and $\mathbf{X_2F}$+$\mathbf{X_2S}$ = orange) indicate the product(s) of each reaction. In the case of SM1, SM2, SM4, and SM5 the reaction results in the **XB** PCC. In SM4 and SM6 the reaction results in a mix of $\mathbf{X_2F}$ and $\mathbf{X_2S}$ PCCs.

Supplement S1: DFT calculations.

All plane-wave density functional theory (DFT) calculations were conducted using the CASTEP module of BIOVIA Materials Studio 2020.[1] Geometry optimization calculations were performed on models based on structures of **X** and PCCs of **X** obtained from single-crystal XRD.[2,3] The revised Perdew-Burke-Ernzerhof (rPBE) functional was used for all geometry optimizations and single-point energy calculations.[4] The plane-wave cutoff energy was 630 eV with a *k*-point spacing of 0.07 $Å^{-1}$.[5] The interaction between core and valence electrons was modeled using the ultrasoft pseudopotentials generated on the fly.[6,7] Thresholds for assessing the structural convergence included a maximum change in energy of 5×10^{-6} eV per atom, a maximum displacement of 5×10^{-4} Å per atom, and a maximum Cartesian force of 0.01 eV $Å^{-1}$. The unit cell was fixed all calculations and dispersion was included in the structural refinements through a reparameterization of damping function in the semi-empirical two-body force field model of Grimme ($s_6 = 1.00$ and $d = 3.5$).[8–12]

Static lattice energies were obtained from calculations on geometry optimized models of the solids. All the systems are binary PCCs with composition M_aN_b, where M represents the API (*i.e.,* **X**), *N* represents the coformer (*i.e.,* **B**, **F**, or **S**), and *a* and *b* represent the stoichiometric amounts of API and coformer, respectively. The enthalpy of cocrystallization is defined by:

$$\Delta H_{cc}(M_aN_b) = H_{tot}(M_aN_b) - [aH_{tot}(M) + bH_{tot}(N)] \quad (1)$$

where $H_{tot}(M_aN_b)$, $H_{tot}(M)$, and $H_{tot}(N)$ are the static lattice energies for the crystal structures of the PCC, API, and coformer, respectively.[13,14]

References

1 S. J. Clark, M. D. Segall, C. J. Pickard, P. J. Hasnip, M. I. J. Probert, K. Refson and M. C. Payne, *Z. Kristallogr. - Crystalline Materials*, 2005, **220**, 567–570.

2 D. W. Robertson, N. D. Jones, J. K. Swartzendruber, K. S. Yang and D. T. Wong, *J Med Chem*, 1988, **31**, 185–189.

3 S. L. Childs, L. J. Chyall, J. T. Dunlap, V. N. Smolenskaya, B. C. Stahly, G. P. Stahly, A. v Kent, W. Lafayette and B. Road, *J Am Chem Soc*, 2004, **126**, 13335–13342.

4 B. Hammer, L. B. Hansen and J. K. Nørskov, *Phys Rev B*, 1999, **59**, 7413–7421.

5 H. J. Monkhorst and J. D. Pack, *Phys Rev B*, 1976, **13**, 5188–5192.

6 J. R. Yates, C. J. Pickard and F. Mauri, *Phys Rev B Condens Matter Mater Phys*, 2007, **76**, 1–11.

7 J. R. Yates, C. J. Pickard, M. C. Payne and F. Mauri, *Journal of Chemical Physics*, 2003, **118**, 5746–5753.

8 S. T. Holmes and R. W. Schurko, *The Journal of Physical Chemistry C*, 2018, **122**, 1809–1820.

9 S. T. Holmes, R. J. Iuliucci, K. T. Mueller and C. Dybowski, *J Chem Phys*, 2017, **146**, 064201.

10 S. Grimme, *J Comput Chem*, 2006, **27**, 1787–1799.

11 A. A. Peach, D. A. Hirsh, S. T. Holmes and R. W. Schurko, *CrystEngComm*, 2018, **20**, 2780–2792.

12 E. R. McNellis, J. Meyer and K. Reuter, *Phys Rev B*, 2009, **80**, 205414.

13 G. Sun, Y. Jin, S. Li, Z. Yang, B. Shi, C. Chang and Y. A. Abramov, *Journal of Physical Chemistry Letters*, 2020, **11**, 8832–8838.

14 C. R. Taylor and G. M. Day, *Cryst Growth Des*, 2018, **18**, 892–904.